*Journal of the Meteorological Society of Japan*, Vol. 77, No. 6, pp. 1123–1136, 1999 

# Disturbances of 1–2 Hour-Periods Observed in the Tropical Lower Troposphere during the TOGA-COARE IOP

**By Shoichi Shige**

*Disaster Prevention Research Institute, Kyoto University, Kyoto, Japan*

*(Manuscript received 19 August 1998, in revised form 6 August 1999)*

## Abstract

Mesoscale disturbances in the tropical lower troposphere having periods of 1–2 hours were detected in the wind profiler data during the intensive observing period of the Tropical Ocean-Global Atmosphere Coupled Ocean-Atmosphere Response Experiment (TOGA-COARE). Seven cases were detected with average amplitudes of the vertical velocity greater than 0.1 m $s^{-1}$.

One case that was observed at Kapingamarangi (1.1°N, 154.8°E) on January 7, 1993 was examined in detail. This disturbance had a period of 60 minutes and a duration of 6 hours. Assuming that this disturbance was a gravity wave, the vertical and horizontal wavelengths were estimated as 5.4–7.6 km and 24–37 km, respectively. Using satellite and sounding data, it was inferred that the disturbance was excited by a mesoscale cloud line lying about 400 km ESE from Kapingamarangi, and then propagated in a wave duct in the troposphere.

## 1. Introduction

Recent studies of aircraft observations in the tropical stratosphere have shown that mesoscale gravity waves with periods ranging from a few minutes to a few hours, and with horizontal scales in the 10–100 km range, are associated with convection. Pfister *et al.* (1993) examined a vertically propagating wave with a horizontal wavelength of about 110 km, generated by a tropical cyclone. Alexander and Pfister (1995) observed vertical fluxes of horizontal momentum carried by mesoscale gravity waves on both sides of a tropical cloud band. They determined that gravity waves with horizontal scales of 10–100 km propagated from a tropical cloud band.

Mesoscale gravity waves with periods of 1–4 hours, and horizontal wavelengths of 50–500 km, have been frequently observed in association with intense mesoscale convective systems. These waves were observed in the extratropical troposphere, with abundant data having time resolution fine enough to resolve them (Uccellini and Koch, 1987). Recently, Ralph *et al.* (1993) observed a mesoscale gravity wave having a 90-min period, using a 50-MHz radar wind profiler and data from 19 automated surface observation stations in southwestern France during the summer of 1984. It was concluded that the wave propagated via a wave duct between the ground and about 4.5 km, by the mechanism proposed by Lindzen and Tung (1976).

In contrast to the tropical stratosphere, and the extratropical troposphere, mesoscale gravity waves have hardly been reported in the tropical troposphere. There may be three reasons for this: 1) it is more difficult to separate internal gravity waves from the background flow in the troposphere than it is in the stratosphere, 2) if there is no mechanism for trapping wave energy in the troposphere, mesoscale gravity waves are not detectable far from their source in the troposphere, since they propagate vertically into the middle atmosphere, 3) data with time resolution fine enough to resolve mesoscale waves have been very scarce in the tropical troposphere compared with data from the extratropical troposphere.

The importance of the interaction between the gust front of a convective cell and the background low-level shear has been known for the development of intense squall lines. Rotunno *et al.* (1988) suggested that a convective cell is more vertically ori-

Corresponding author and present affiliation: Shoichi Shige, Division of Earth and Planetary Sciences, Graduate School of Science, Kyoto University, Kyoto 606-8502, Japan. E-mail: shige@kugi.kyoto-u.ac.jp

ented and intense when the background low-level shear is of the opposite sign, but equal in magnitude to the vorticity produced by buoyancy gradients across the gust front of a convective cell. In the tropics, however, there are instances when convective lines form in environments without appreciable low-level shear. For example, the slow-moving tropical cloud lines studied by Barnes and Sieckman (1984) developed without appreciable low-level shear. Furthermore, Parsons *et al.* (1994) reported that the cold pool is shallow over the tropical ocean. Besides the interaction of the gust front of a convective cell with the background low-level shear, cooperation between convective cells and gravity waves in the troposphere is known as a mechanism for self-organizing convection. Schmidt and Cotton (1990), using a two-dimensional numerical model, demonstrated that gravity waves determine the propagation speed of a squall line and are instrumental in lifting low-level air to the level of free convection. In the tropics, it is expected that interaction between convective cells and gravity waves is more important than cold-pool dynamics as the self-organizing mechanism of convection.

The purpose of the present study is to detect mesoscale disturbances having periods ranging from a few minutes to a few hours in the tropical troposphere. Data were obtained by the 915-MHz wind profilers continuously operated during the Tropical Ocean-Global Atmosphere Coupled Ocean-Atmosphere Response Experiment (TOGA-COARE), Intensive Observing Period (IOP) (Webster and Lukas, 1992). This was conducted from 1 November 1992 to 28 February 1993 in the western equatorial Pacific region. The disturbances were further analyzed using upper-atmospheric soundings, surface meteorological data, and satellite data obtained during the TOGA-COARE IOP.

## 2. Data and method of analysis

The data used in the present study were provided by the 915-MHz wind profilers, deployed over the tropical western pacific during the TOGA-COARE IOP as a part of the network of Integrated Sounding Systems (ISSs) (Parsons *et al.*, 1994). The data were those observed by profilers deployed on three ISS-island sites: Kapingamarangi (1.1°N, 154.8°E, LT = UTC + 10 h 20 m), Kavieng (2.6°S, 150.8°E, LT = UTC + 10 h 00 m), and Manus Island (2.1°S, 147.4°E, LT = UTC + 09 h 50 m). Each station was separated by more than 300 km, as shown in Fig. 1. The temporal resolution of the profiler data was about 4 minutes. The observed heights ranged from 0.1 km to about 4 km. The vertical resolution was 255 m. The maximum observation height depended on atmospheric conditions. The vertical velocity data during rain events were excluded, since the wind profilers also observed the fall velocity of precipitating particles. Downward velocity data of greater than 2.0 m $s^{-1}$ were also removed. They were thought of indicating the fall velocities of precipitating particles, even though it was not raining at the surface. Details of the system of ISS wind profilers were given by Parsons *et al.* (1994), Miller and Riddle (1994), and Gage *et al.* (1994).

Use was also made of four times daily, upper-atmospheric sounding data obtained from the ISS at six stations—Kapingamarangi, Kavieng, Manus, Nauru (0.5°S, 166.9°E), and the research vessel (R/V) Shiyan (2.2°S, 158.0°E). For the surface data, ISS surface observations with one-minute temporal resolutions at Kapingamarangi, Kavieng, and Manus were utilized. To obtain information concerning cloud systems, the infrared equivalent blackbody temperature data $T_{BB}$ over the TOGA-COARE region were utilized. These were observed by the Japanese Geostationary Meteorological Satellite (GMS/IR). The spatial and temporal resolution of the GMS/IR $T_{BB}$ are 0.1° × 0.1°, and 1 hour.

In order to find successive wavelike disturbances and determine their duration, the high-frequency noise was removed from the time series of the vertical velocity data observed by the wind profilers. A Lanczos low-pass filter (Duchon, 1979) with a cut-off length of 28 minutes, and a filter length of 168 minutes, was applied to remove the high-frequency noise. When successive wavelike disturbances were found, power spectral densities were calculated for the unfiltered time series of the vertical velocity data to determine the dominant period for each case. In order to calculate the power spectral densities, the Fast Fourier Transform (FFT) method was applied to the unfiltered time series of the vertical velocity data for the time span including the duration of the wave disturbance for each case. In order to extract the dominant period for each case, the Lanczos bandpass filtering was then applied to the unfiltered vertical velocity time series. The bandwidths of the Lanczos bandpass filter were chosen to maintain the power of the oscillation with its determined dominant period.

Following the above procedure, seven cases of wave disturbances were selected under conditions that the time-height average of the vertical velocity amplitudes was nearly equal to, or greater than, 0.1 m $s^{-1}$, and the wave duration lasted for more than four cycles.

## 3. Results

### *3.1 Characteristics of 1–2 hour-period disturbances*

The seven cases detected in the present study are listed in Table 1. The observed periods in Table 1 were determined by spectral analysis (see Figs. 2(a)–(g)). For the FFT analyses, the vertical velocity time series data (8 hours), which included the wave

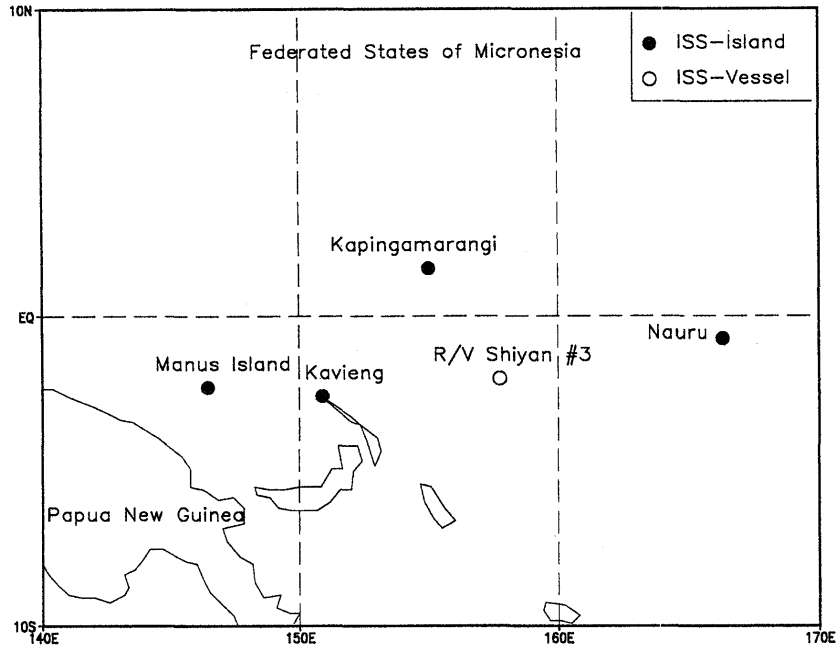


Fig. 1. Map of TOGA-COARE ISS sites where data used in the present study were observed.

Table 1. Observed 1–2 hour-period disturbances. Observational sites Manus, Kavieng, and Kapingamarangi are abbreviated as Man, Kav, and Kap, respectively.

| Case | Site | Date | UTC | Observed Period | Life Time | $\overline{\lvert w' \rvert}$ | type |
|---|---|---|---|---|---|---|---|
| A | Man | 3 Jan 1993 | 15–23 | 120 min | 8 h | 0.12 m s$^{-1}$ | II |
| B | Man | 5 Jan 1993 | 04–09 | 69 min | 4 h | 0.13 m s$^{-1}$ | III |
| C | Kav | 13 Jan 1993 | 10–17 | 60 min | 7 h | 0.098 m s$^{-1}$ | |
| D | Kav | 23 Jan 1993 | 11–16 | 69 min | 5 h | 0.11 m s$^{-1}$ | III |
| E | Kap | 15 Dec 1992 | 18–24 | 53 min | 6 h | 0.10 m s$^{-1}$ | |
| F | Kap | 7 Jan 1993 | 16–22 | 60 min | 6 h | 0.12 m s$^{-1}$ | I→II |
| G | Kap | 10–11 Jan 1993 | 21–05 | 120 min | 8 h | 0.12 m s$^{-1}$ | II |

duration for each case, were used after the application of the 20 % cosine-taper window. Figure 2(h) shows the ensemble average of the seven cases. The vertical bar in Fig. 2(h) indicates the 95 % confidence limit. Pressure oscillations could not be detected over the same period range as the vertical velocity oscillation. This point will be discussed in a later section.

Six cases out of the seven were observed to occur around 01–09 LT. Chen and Houze (1997) reported that cloud clusters with maximum size exceeding 300 km reached maximum areal extent during the night and early morning hours. Time clustering of the observed cases may be related to the diurnal cycle of the convective activity, although the number of cases is too small to statistically discuss this point.

To examine the structure of the disturbances, the waves with periods of 53 minutes (Case E), 60 minutes (Cases C and F), and 69 minutes (Cases B and D) were extracted by using a bandpass filter with cutoff periods of 36 and 84 minutes. The waves having 120 minute periods (Cases A and G) were extracted using a bandpass filter with cutoff periods of 96 and 144 minutes. The response functions for the Lanczos bandpass filters are plotted in Fig. 3.

Figure 4 shows the time-height cross sections of vertical velocity for the seven cases listed in Table 1. The vertical phase structures have various types. Several disturbances indicate a downward phase propagation (Cases B and D), or no vertical propagation (Cases A and G). Time variation of the vertical structure (Case F) can be seen. This exhibits an upward phase propagation in the earlier stage (16–19 UTC), and a standing wave in the latter stage (19–22 UTC). The phases of Cases C and E are not clearly seen.

*3.2 Parameter estimation*

A linear gravity wave theory with the Boussinesq approximation is used to estimate the wave parameters. Figure 5 schematically illustrates the structures of two-dimensional, monochromatic grav-

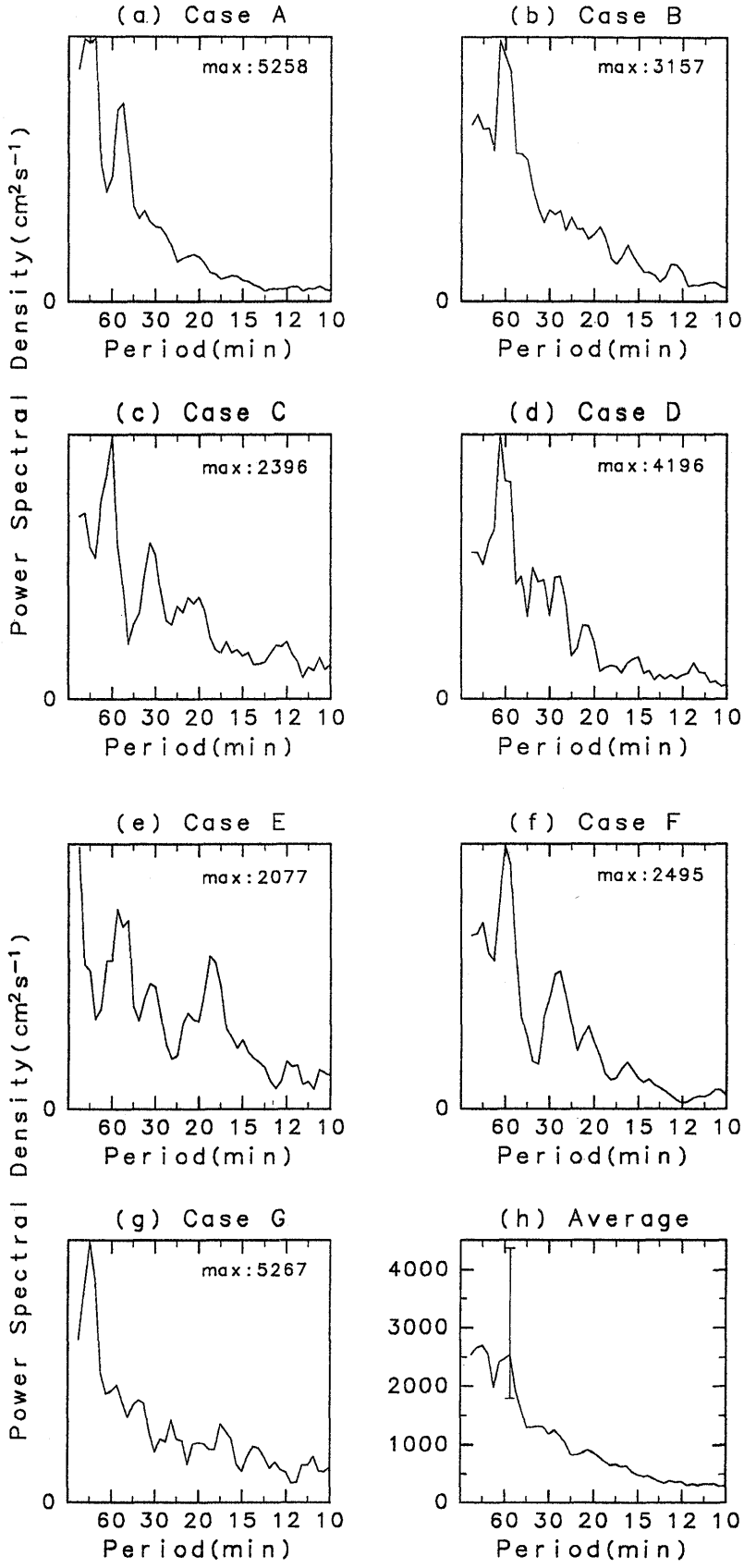


Fig. 2. (a)–(g) Power spectra of the vertical velocity observed by profilers for each case listed in Table 1. The linear vertical scales have been normalized by each maximum spectral density indicated in each figure. (h) The ensemble average of the seven cases. The vertical bar indicates the 95 % confidence limit.

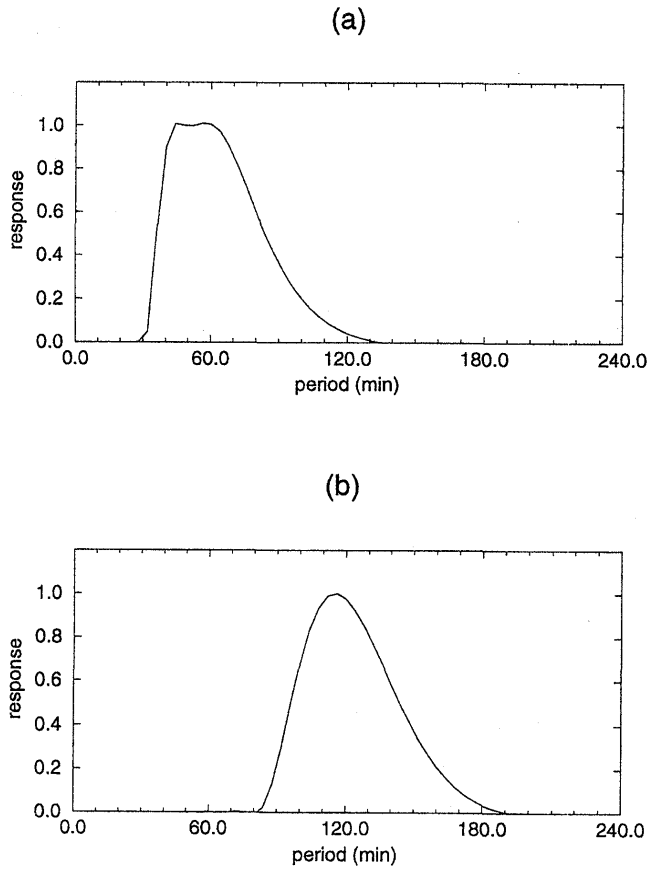


Fig. 3. The response functions for the Lanczos filter with cutoff periods of (a) 36 minutes and 84 minutes, and (b) 96 minutes and 144 minutes.

ity waves which are totally reflected at the surface. For the present purposes, a gravity wave is considered and assumptions are made that:

$$w' = \hat{w}e^{i(kx+mz-\omega t)},$$
$$u' = \hat{u}e^{i(kx+mz-\omega t)}, \quad (1)$$

where $u'$ is horizontal wind perturbation, $\hat{w}$ and $\hat{u}$ are wave amplitudes. Here, $x$ is chosen parallel to the direction of wave propagation in the horizontal plane, $k$ is the horizontal wave number ($k > 0$), $m$ the vertical wave number, and $\omega$ the observed frequency. Lines of constant phase $\phi = kx + mz$ tilt as Type I, shown in Fig. 5 for $m > 0$, and as Type III for $m < 0$. A standing wave such as Type II can be seen in the region where Type I and Type III interfere with each other.

In the time-height cross sections of waves observed at a fixed station, the Type I wave is expected to exhibit upward phase propagation, the Type II wave no vertical propagation of phase, and the Type III wave downward phase propagation. The types of the seven cases examined in the present study are determined as shown in Table 1. The phases in the time-height cross sections of Cases C and E are not clear (Figs. 4(c) and (e)). The vertical phase structures of Cases B and D shown in Figs. 4(b) and (d) are Type III, suggesting that the waves propagate energy upward. The vertical phase structures of Cases A and G shown in Figs. 4(a) and (g) are type II, which suggests wave reflection at the surface. As shown in Fig. 4(f), the vertical structure over the first-half of wave duration (16–19 UTC) for Case F is Type I, suggesting that the wave propagates energy downward. On the other hand, the structure over the second-half of wave duration (19–22 UTC) of Case F is Type II, which suggests wave reflection at the surface.

Using the continuity equation for a linear monochromatic wave

$$ku' + mw' = 0, \quad (2)$$

the relationship between $w'$ and $u'$ can be expressed as

$$u' = -w'\frac{m}{k}. \quad (3)$$

The horizontal direction of wave propagation for Type I and III cases can be determined from this relationship. The absolute value of the correlation coefficient (AVCC) between the vertical velocity and the horizontal wind $|\overline{u_\theta w'}|$ is utilzed. The horizontal direction of wave propagation is the direction

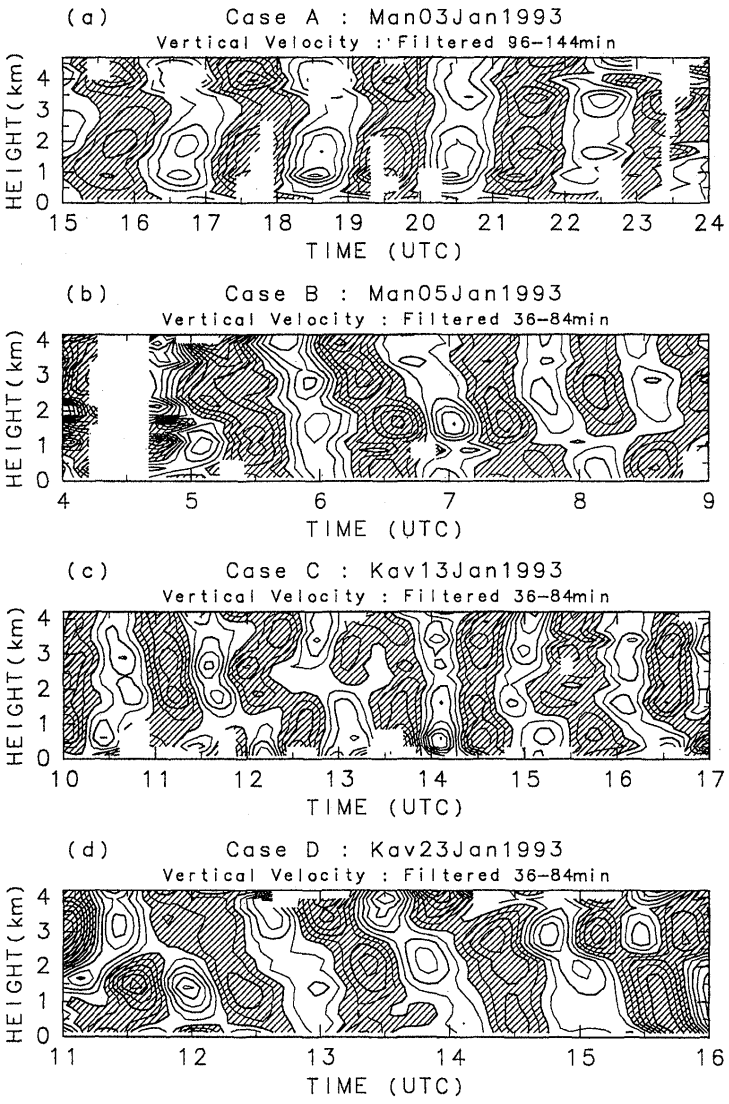


Fig. 4. Time-height cross sections of the vertical velocities of the 1–2 hour-period wave disturbances. The contour interval is 0.05 m $s^{-1}$. Shaded regions indicate downward velocity.

in which $|\overline{u_\theta w'}|$ has the maximum value. Here, $u_\theta$ is the horizontal wind in the direction of $\theta$. The direction of $\theta$ is determined clockwise from north. The over-bars denoted the time-height mean over the observed height range and wave duration. The directions when $-\overline{u_\theta w'}$ are maximum for the Type I (Case F), and those when $\overline{u_\theta w'}$ are maximum for the Type III (Cases B and D), are determined by calculating $\overline{u_\theta w'}$ at 1°-intervals over 360°.

For Cases B and D, which were determined as Type III, the absolute value of the correlation coefficient (AVCC) between the vertical velocity and horizontal winds is less than 0.7. For Case F, the AVCC between the vertical velocity (Fig. 6(a)) and horizontal winds (Fig. 6(b)) in the first half (16–19 UTC) has a maximum value of 0.78 in the direction ($\theta = 287°$). The determination of wave propagation requires that the maximum AVCC between the vertical velocity and horizontal winds must be larger than the criterion value of 0.7. Therefore the horizontal direction of wave propagation can only be determined for Case F, where the AVCC between the vertical and horizontal winds is the largest. The AVCC between the vertical velocity (Fig. 6(a)) and horizontal winds in the direction perpendicular to the detected direction of wave propagation (Fig. 6(c)), is 0.05. The amplitudes of the horizontal wind in the direction perpendicular to the detected direction of wave propagation (Fig. 6(c)), are smaller than those in the detected direction of wave propagation (Fig. 6(b)). This supports the assumption that this disturbance is a plane gravity wave.

For Case F, where the direction of wave propagation could be determined, the wave parameters can be estimated from the linear dispersion relation for

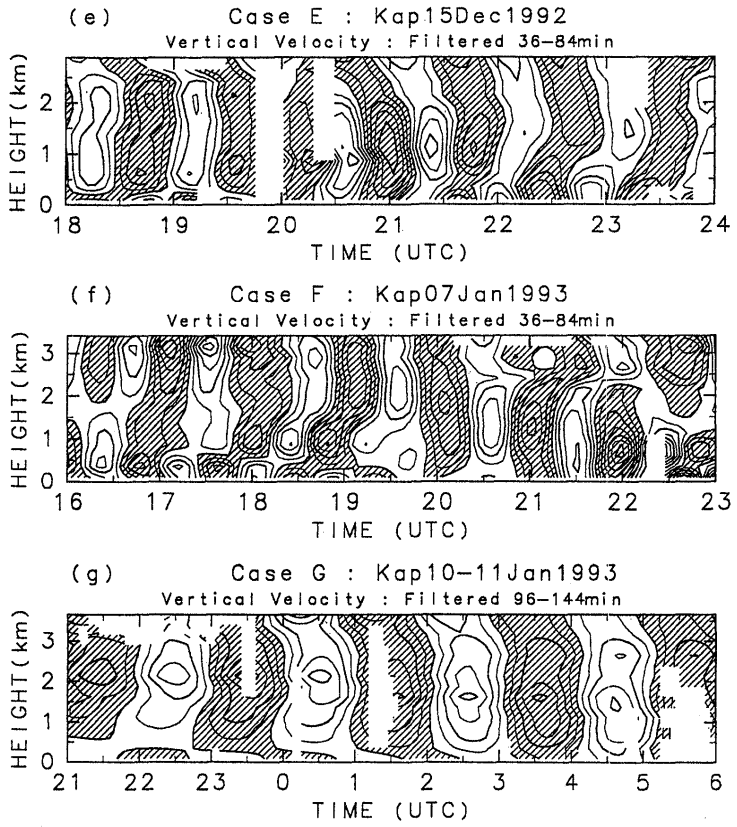


Fig. 4. (Continued).

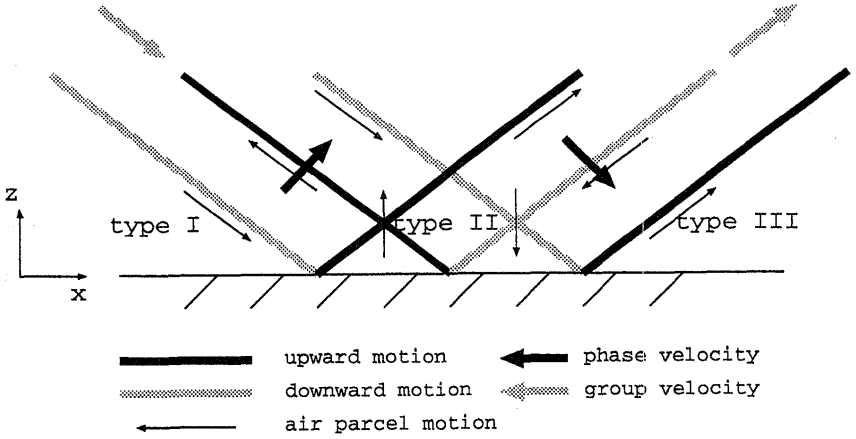


Fig. 5. Schematic illustration of several types of internal gravity waves reflected at the surface.

internal gravity waves as

$$\hat{\omega} \equiv \omega - Uk = \frac{Nk}{\sqrt{k^2 + m^2}}, \tag{4}$$

where $\hat{\omega}$ is the intrinsic frequency, $\omega$ the observed frequency, $U$ the background wind speed in the direction of the wave propagation, and $N$ the Brunt-Väisälä frequency. The estimated variables $T(= 2\pi/\omega)$, $U$, and $N$ are listed in the middle column of Table 2. From the soundings at Kapingamarangi at 1800 UTC on 7 January, $U$ is obtained by averaging the wind speeds in the direction of the phase propagation from the surface to the maximum observation height of the disturbance. The Brunt-Väisälä frequency $N$ is also determined from the soundings at the surface to the maximum observation height of the disturbance.

The vertical wavelength $L_z$ is calculated as 5.4–7.6 km from

$$L_z = 2\pi/m = \frac{2\pi c_z}{\omega}, \tag{5}$$

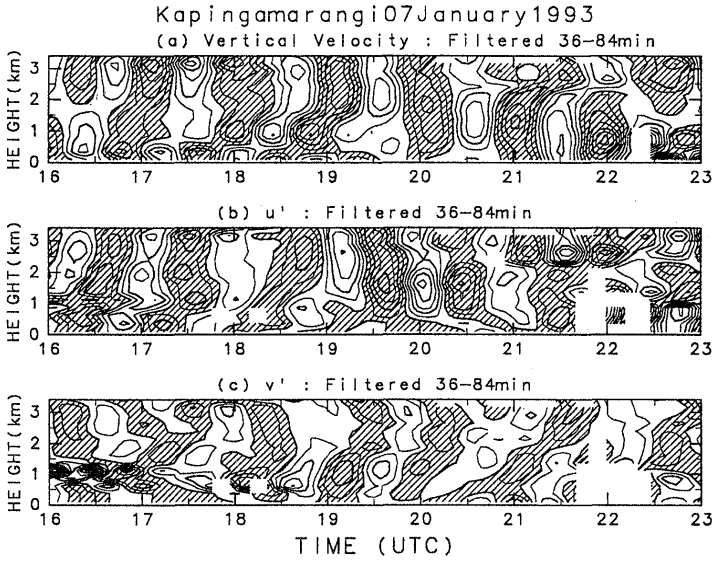


Fig. 6. Time-height cross sections of (a) vertical velocities, (b) horizontal wind $u'$ in the phase propagation direction, and (c) horizontal wind $v'$ in the direction 90° counterclockwise to the horizontal wave propagation direction. The contour intervals are 0.05 m s$^{-1}$, and 0.2 m s$^{-1}$ for vertical and horizontal winds, respectively. Shaded regions indicate negative values.

Table 2. Observed wave parameters for Case F. In the middle column, the values of $T$, $c_z$, $U$, and $N$ calculated in Sec. 3.2 are listed, while those calculated in Sec. 4.1 are listed in the right-hand column. Note that the values of $T$ and $c_z$ in Sec. 3.2 and Sec. 4.1 are identical.

| | Sec. 3.2 | Sec. 4.1 |
|---|---|---|
| $T(=2\pi/\omega)$ | 60 min | 60 min |
| $c_z$ | 1.7 to 2.4 m s$^{-1}$ | 1.7 to 2.4 m s$^{-1}$ |
| $U$ | −2.5 m s$^{-1}$ | −1.7 m s$^{-1}$ |
| $N$ | 0.012 s$^{-1}$ | 0.010 s$^{-1}$ |

where $c_z$ is the vertical phase speed. The estimated variable $c_z$ is listed in the middle column of Table 2. The vertical phase speed, $c_z$, is estimated from three cycles occurring in the first half of Type I. Substituting the obtained parameters $\omega, m, U$, and $N$ into Eq. (4), and using the condition that $k$ and the horizontal group velocity are positive, the horizontal wavelength $L_x(=2\pi/k)$ is estimated as 27–42 km. From these estimated values, the intrinsic period

$$\hat{T}(=2\pi/\hat{\omega}), \tag{6}$$

the horizontal phase velocity relative to the ground

$$c_x = \frac{\omega}{k}, \tag{7}$$

the horizontal group velocity

$$c_{gx} = \frac{\partial\omega}{\partial k} = U + \frac{Nm^2}{(k^2+m^2)^{3/2}}, \tag{8}$$

Table 3. Estimated wave parameters for Case F. In the middle column, the values of $\hat{T}$, $L_x$, $L_z$, $c_x$, $c_{gx}$, and $c_{gz}$ estimated in Sec. 3.2 are listed, while those estimated in Sec. 4.1 are listed in the right-hand column. Note that the values of $L_z$ estimated in Sec. 3.2 and Sec. 4.1 are identical.

| | Sec. 3.2 | Sec. 4.1 |
|---|---|---|
| $\hat{T}(=2\pi/\hat{\omega})$ | 45 to 50 min | 47 to 51 min |
| $L_x(=2\pi/k)$ | 27 to 42 km | 24 to 37 km |
| $L_z(=2\pi/m)$ | 5.4 to 7.6 km | 5.4 to 7.6 km |
| $c_x$ | 7.6 to 12 m s$^{-1}$ | 6.7 to 10 m s$^{-1}$ |
| $c_{gx}$ | 7.2 to 11 m s$^{-1}$ | 6.3 to 9.7 m s$^{-1}$ |
| $c_{gz}$ | −1.9 to −2.5 m s$^{-1}$ | −1.8 to −2.4 m s$^{-1}$ |

and the vertical group velocity relative to the ground

$$c_{gz} = \frac{\partial\omega}{\partial m} = -\frac{Nkm}{(k^2+m^2)^{3/2}}, \tag{9}$$

are estimated. The results are listed in the middle column of Table 3.

## 4. Discussion

### *4.1 Trapping and wave source*

Convection has the ability to generate short-period (< 1 day) gravity waves with small horizontal scales in the 10–100 km range (Sato, 1997). Convection is most likely the source of the mesoscale disturbances of 1–2 hour-periods in the tropical lower troposphere observed in the present study. Figure 7

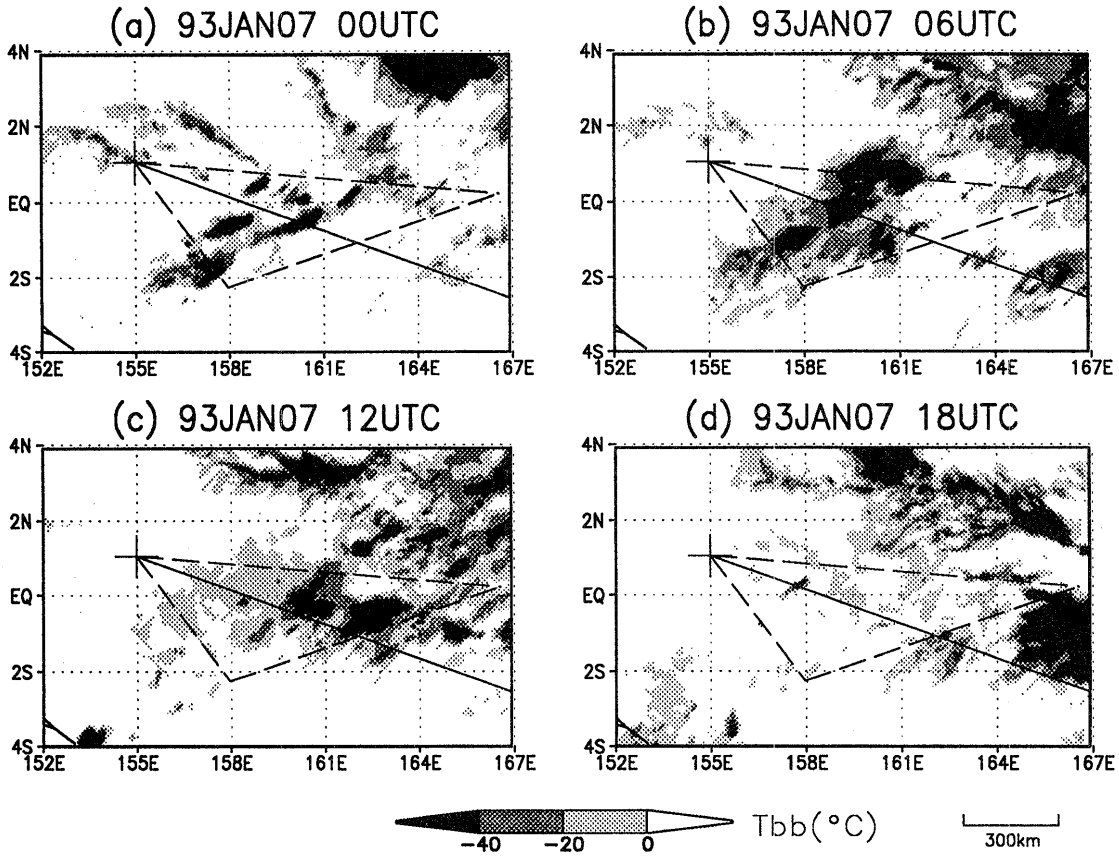


Fig. 7. Sequence of $T_{BB}$ infared image maps around Kapingamarangi at (a) 0000 UTC, (b) 0600 UTC, (c) 1200 UTC, and (d) 1800 UTC on January 7. The plus symbols (+) indicate the location of Kapingamarangi, and the solid lines indicate the direction of the wave source. The dotted lines indicate the triangle that consists of three stations (Kapingamarangi, R/V Shiyan and Nauru) for which the average horizontal divergence was computed. The degree of shading denotes the range of $T_{BB}$ temperatures, as indicated by the value bar at the bottom of the figure. The horizontal scale is also indicated at the lower right.

presents a sequence of $T_{BB}$ maps from the GMS infrared images for 00 UTC to 18 UTC on January 7 around Kapingamarangi, where Case F was observed. The direction of the wave source is 107° (clockwise from north), because the direction of the wave propagation was determined as 287° (clockwise from north) in the previous section. The mesoscale cloud line (MCL) is located about 400 km from Kapingamarangi in the direction of approximately 107° clockwise from north. It is inferred that Case F was excited by the MCL, which is located about 400 km ESE from Kapingamarangi.

If there is no mechanism for trapping wave energy in the troposphere, tropospheric gravity waves excited by the MCL would normally propagate into the middle atmosphere before reaching Kapingamarangi. Lindzen and Tung (1976) proposed four conditions necessary for a duct in which gravity waves can be trapped: 1) a statically stable layer, in which gravity waves could propagate, is adjacent to the ground, 2) the duct is deeper than one quarter of the vertical wavelength, 3) the duct is topped by an unstable layer of Richardson number $Ri\left(=N^2/\left(\frac{dU}{dz}\right)^2\right) < 0.25$, and 4) the unstable layer contains a critical level where the mean wind speed is equal to, or nearly equal to the ground-relative phase speed of the gravity wave.

Figure 8 shows the vertical profiles of $U$, $\left(\frac{dU}{dz}\right)^2$, $N^2$, and $Ri$ calculated using winds, temperature, and humidity obtained by ISS radiosondes. These were at the following ISS sites near the propagation path of the disturbance: Kapingamarangi, R/V Shiyan, and Nauru at 12 UTC (before the passage of the wave), and Kapingamarangi and R/V Shiyan at 18 UTC (during the passage of the wave) on January 7. The vertical profiles of $U$, $\left(\frac{dU}{dz}\right)^2$, $N^2$, and $Ri$ for Nauru at 18 UTC were not calculated because sounding data above 5 km were not available. From Fig. 8, it can be seen that the profiles of $N^2$ from the surface to 13 km are favorable for wave ducting. The mean wind speeds at 13–14 km at 12 UTC and 18 UTC are almost equal to the ground-relative

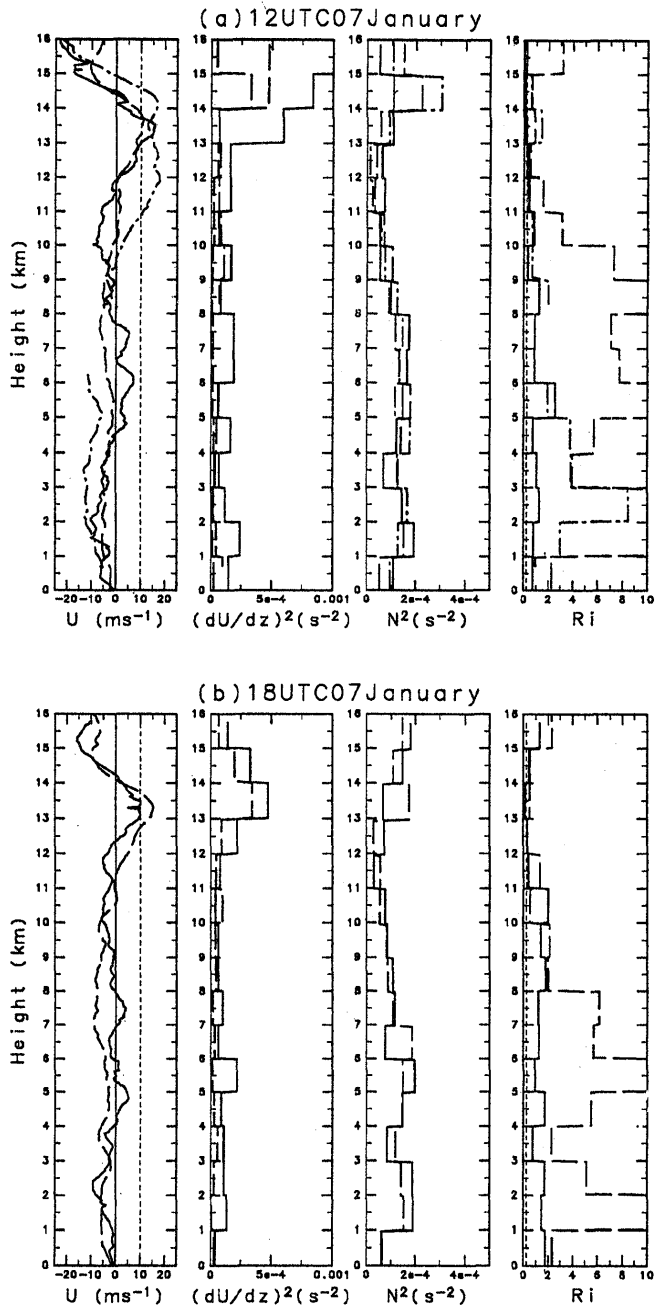


Fig. 8. Vertical profiles of horizontal wind in the phase propagation direction $U$ (ms$^{-1}$), square of the vertical shear of horizontal wind $(\frac{dU}{dz})^2$ (s$^{-2}$), square of the Brunt-Väisälä frequency $N^2$ (s$^{-2}$), and the Richardson number $Ri$ deduced from soundings at Kapingamarngi (solid lines), R/V Shiyan (long dashed lines), and Nauru (dash dotted lines). The profiles are shown for (a) before (1200 UTC on 7 January), and (b) during (1800 UTC on 7 January) the passage of the disturbance. The thin solid lines and dashed lines in the vertical profiles of $U$ mark wind speeds of zero and 10.0 m s$^{-1}$ (the phase speed of the wave), respectively. Short dashed line in the vertical profiles indicate the Richardson number value of 0.25.

phase speed of the disturbance (about 10.0 m s$^{-1}$). In addition, the layer from 13 to 14 km is unstable, *i.e.*, $Ri < 0.25$ at 12 UTC and 18 UTC. These characteristics meet the conditions for a wave duct as discussed by Lindzen and Tung (1976). Therefore the disturbance was possibly excited by the MCL and propagated in the duct between the sea surface and the 13 km level.

The estimation of parameters in Section 3.2 depended on $U$ and $N$. In Section 3.2, wave parame-

ters were estimated using $U$ and $N$ obtained by averaging horizontal wind speeds in the direction of the phase propagation, and the Brunt-Väisälä frequency from the surface to the maximum observation height of the disturbance. Since it is inferred that the disturbance propagated in the duct between the sea surface and the 13 km level, wave parameters should be re-estimated using $U$ and $N$ calculated by averaging those in the 0–13 km height range. The calculated $U$ and $N$ are listed in the right-hand column in Table 2. Wave parameters estimated using these values of $U$ and $N$ are listed in the right-hand column in Table 3. Re-estimated $c_x$ (about 8.0 m s$^{-1}$) varies only slightly from the $c_x$ estimated in Section 3.2, so that the characteristics of the layer from 13 to 14 km still meet the fourth condition of a wave duct as discussed by Lindzen and Tung (1976). For the re-estimated wave parameter, it is also concluded that the disturbance could propagate horizontally about 400 km in the troposphere. The estimated group velocity $c_{gx}$ of approximately 8.0 m s$^{-1}$ indicates that the disturbance takes about 14.0 hours to propagate from the MCL to the observation site at Kapingamarangi (about 400 km).

The mesoscale convective system suggested as the wave source has a line shape as seen in Fig. 7. Generally, waves excited by a line source will propagate farther, compared with waves excited by a point source. This results from the fact that the energy density of waves excited by a point source decreases according to the inverse of the radius from the source, while the energy density of waves excited by a line source does not decrease. Thus, the two-dimensionality of the mesoscale convective system assumed as the source appears to be favorable for the horizontal propagation of the wave.

There are two reasons why the Case F disturbance was observed at Kapingamarangi: 1) it is a favorable location for the duct, since Kapingamarangi is located in the direction where the third and the fourth ducting conditions discussed by Lindzen and Tung (1976) are satisfied; 2) the region is favorable for the horizontal propagation of the wave, since Kapingamarangi is located in the ray path of the observed wave, which crosses the center of the MCL nearly perpendicularly. The Case F disturbance was not observed at Kavieng or Manus Island, because at these observation sites two conditions mentioned above were not met. After examining the GMS infrared images, it was apparent that this wave did not seem to excite new convection.

*4.2 Horizontal divergence profiles in MCL*

Figure 9 shows the horizontal divergence profiles in the MCL. The average horizontal divergence was computed using radiosonde data at 00 UTC, 06 UTC, 12 UTC, and 18 UTC on January 7 in the triangle formed by the three stations (Kapingamarangi, R/V Shiyan, and Nauru). These stations surround the MCL as shown in Fig. 7. A linear variation of the wind was assumed between triangle vertices. From Figs. 9(a) and (b), convergence occurs between 950 and 600 hPa. In Figs. 9(c) and (d), convergence is detected between 750 and 550 hPa, with divergence at lower levels.

Mapes and Houze (1995) examined the horizontal divergence measured with airborne Doppler radar inside ten mesoscale convective systems observed during the TOGA-COARE. It was found that young convective systems have near-surface convergence, while mature cells with better-developed downdrafts and stratiform precipitation areas exhibit peak convergence aloft.

As mentioned in Figs. 9(a) and (b), convergence is found in the lower troposphere. With consideration of the results of Mapes and Houze (1995), the MCL was probably in the growing stage of its life cycle from 00 UTC to 06 UTC, consisting of towers of young growing cumulonimbus. On the other hand, Figs. 9(c) and (d) exhibit divergence in 750–900 hPa layer with convergences at the 0°C isotherm level (~560 hPa). This suggests that from 12 UTC to 18 UTC, the MCL was in its decaying stage of the life cycle, consisting of stratiform precipitation. The convergence in Figs. 9(c) and (d) is considered to correspond to the melting convergence as discussed by Mapes and Houze (1995), characterizing the divergence in the stratiform region. It is inferred that when the MCL was in the growing stage it excited the Case F disturbance from 02 UTC to 08 UTC, and then shifted to the decaying stage. The Case F disturbance may have been excited by a multicell storm within the MCL. The six cycles of the Case F disturbance might correspond to the cycles of cell regeneration within the multicell storm.

The dominant period of waves observed far from their source region is probably decided by both the wave forcing and the wave duct, while the waves may have other dominant periods near the source region. Waves with periods close to the time scale of a convective cell (~1 hour, Houze 1993) would be most dominantly excited. Shige and Satomura (1999) investigated the gravity wave response of the troposphere to a convective cell. They demonstrated that shallow vertical mode waves have short periods, while deep vertical mode waves have longer periods. From the linear dispersion relation for gravity waves (Eq. (4)), shallow vertical mode waves have short horizontal wavelengths, and therefore slow horizontal phase speed (Eq. (7)). Deep vertical mode waves have long wavelengths, and fast horizontal phase speed. Slow modes which has critical levels within the duct (between the sea surface and the 13 km level) will be absorbed at the crtical levels. Fast modes, which have no critical level within the 13–14 km layer of $Ri < 0.25$, will propagate energy

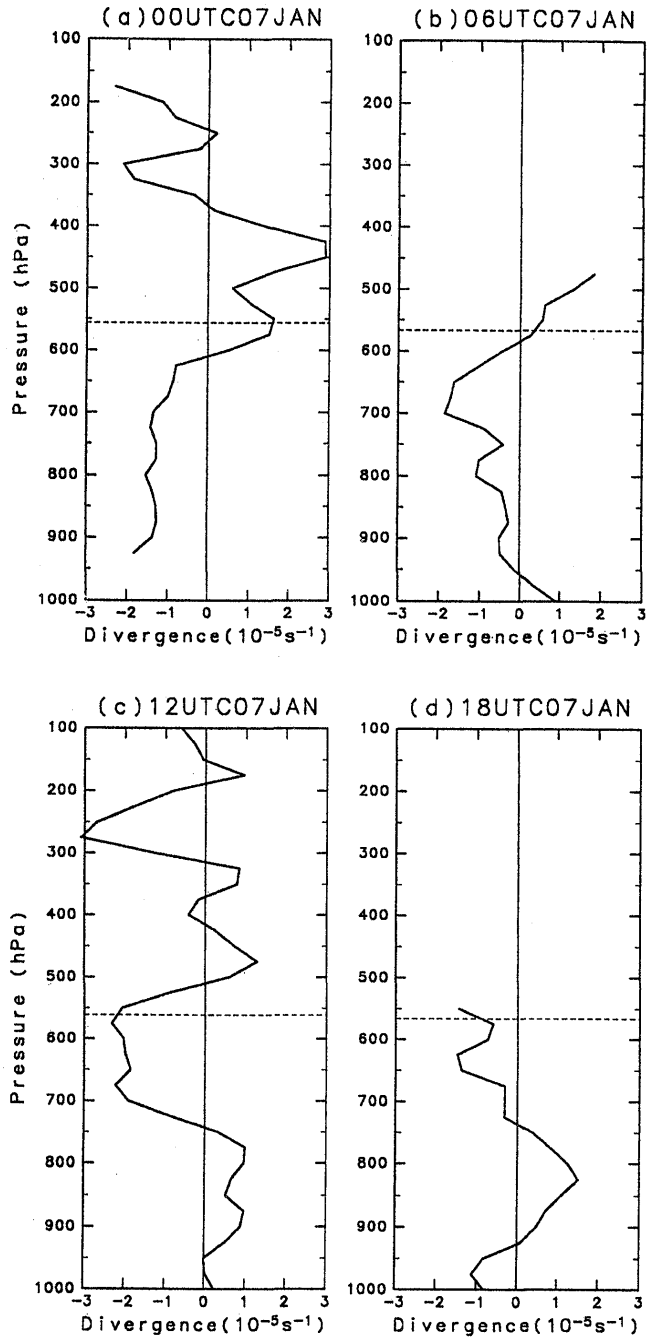


Fig. 9. Averaged horizontal divergence profiles representing the triangle indicated in Fig. 7 at (a) 0000 UTC, (b) 0600 UTC, (c) 1200 UTC, and (d) 1800 UTC on January 7. Horizontal dashed lines indicate the height of the 0°C isotherm.

away from the duct, as suggested by Monserrat and Thrope (1996). As a result, a disturbance with a period of 60 minutes, which has no critical levels within the duct between the sea surface and the 13 km level, and a critical level within the 13–14 km layer of $Ri < 0.25$, would be selected.

*4.3 Surface pressure*

Although the period and the trapping mechanism of the wave observed in the present study were almost the same as those of the gravity wave analyzed by Ralph *et al.* (1993), there was a significant difference in the surface pressure perturbation. Ralph *et al.* (1993) observed a surface pressure oscillation occurring simultaneously, with the same period as the vertical velocity oscillation. In addition, a roughly 90° phase shift was found between the surface pressure oscillation and the velocity oscillation. On the other hand, the present study observed no surface

pressure oscillation. When a gravity wave is totally reflected at the surface, the maximum surface pressure perturbation $|\triangle p_{\max}(0)|$ is given by

$$|\triangle p_{\max}(0)| = \frac{m\omega\rho_0}{k^2}|w_{\max}|, \quad (10)$$

where $\rho_0$ is the mean air density, and $w_{\max}$ the maximum vertical velocity at the antinode. For typical values of $k = 2\pi/31000$ m$^{-1}$, $m = 2\pi/6500$ m$^{-1}$, $\omega = 2\pi/3600$ s$^{-1}$, $|w_{\max}| = 0.2$ m s$^{-1}$ (see Table 2 and 3 and $\rho_0 = 1$ kg m$^{-3}$, the expected surface pressure perturbation $|\triangle p(0)|$ is about 0.082 hPa. This is less than the resolution of the ISS pressure measurement (0.1 hPa). Therfore the pressure perturbation was too small to be resolved in the case of the present study.

## 5. Summary and concluding remarks

Seven cases of disturbances with 1–2 hour-periods were detected in the vertical velocity data from wind profilers operated during the TOGA-COARE IOP (November 1992–January 1993). Assuming that the disturbance was a gravity wave, the vertical and horizontal wavelengths were estimated as 5.4–7.6 km and 24–37 km, for the disturbance observed at Kapingamarangi on 7 January 1993. This disturbance had a 60-minute period and a 6-hour duration. The mesoscale cloud line located about 400 km from Kapingamarangi was considered to be the source of the disturbance. It was suggested from the vertical profiles of divergence that the mesoscale cloud line was in the growing stage when it excited the observed disturbance. The sounding data exhibited a stable layer that was capped by a layer of weak stability and strong vertical wind shear containing a critical level. These conditions were favorable for the trapping and reflection of waves, as discussed by Lindzen and Tung (1976). Thus, it was concluded that the gravity wave could propagate horizontally for approximately 400 km in the troposphere.

## Acknowledgments

The author wishes to express special thanks to Dr. A. Riddle of NOAA, Aeronomy Laboratory for providing the wind profiler data, and to Dr. K. Sato for valuable suggestions. He also wishes to express thanks to Professor H. Muramatsu and Dr. T. Satomura for thoughtful comments and encouragement, and Mr. M. Tanaka, Mr. N. Nishi, Dr. T. Terao, Dr. H. Seko, and Dr. H. Hashiguchi for helpful discussions. Thanks are extended to Dr. Y.N. Takayabu and two anonymous reviewers for their comments on the manusctipt. The GMS data were kindly provided by Dr. T. Nakazawa of the MRI of the Japan Meteorological Agency. This work was partly supported by a research fellowship from the Japan Society for the Promotion of Science for Young Scientists. The GFD-DENNOU and GrADS were utilized for graphics.

## References

Alexander, M.J. and L. Pfister, 1995: Gravity wave momentum flux in the lower stratosphere over convection. *Geophys. Res. Let.*, **22**, 2029–2032.

Barnes, G.M. and K. Sieckman, 1984: The environment of fast- and slow-moving tropical mesoscale convective cloud lines. *Mon. Wea. Rev.*, **112**, 1782–1794.

Chen, S.S. and R.A. Houze, Jr., 1997: Diurnal variation and life-cycle of deep convective systems over the tropical Pacific warm pool. *Quart. J. Roy. Meteor. Soc.*, **123**, 357–388.

Duchon, C.E., 1979: Lanczos filtering on one or two dimensions. *J. Appl. Meteor.*, **18**, 1016–1022.

Gage, K.S., C.R. Williams and W.L. Ecklund, 1994: UHF wind profilers: A new tool for diagnosing tropical convective cloud systems. *Bull. Amer. Meteor. Soc.*, **75**, 2289–2294.

Houze, R.A. Jr., 1993: *Cloud Dynamics*. Academic Press, 573pp.

Lindzen, R.S. and K.K. Tung, 1976: Banded convective activity and ducted gravity waves. *Mon. Wea. Rev.*, **104**, 1602–1617.

Mapes, B.E. and R.A. Houze, Jr., 1995: Diabatic divergence profiles in western Pacific mesoscale convective systems. *J. Atoms. Sci.*, **52**, 1807–1828.

Miller, E.R. and A.C. Riddle, 1994: *TOGA COARE Integrated Sounding System Data Report - vol. IA, Rev. Ed.* TOGA COARE Int. Proj. Off., Univ. Corp. Atmos. Res., Boulder, Colo., 87pp.

Monserrat, S. and A.J. Thorpe, 1996: Use of ducting theory in an observed case of gravity waves. *J. Atmos. Sci.*, **53**, 1724–1736.

Parsons, D., W. Dabberdt, H. Cole, T. Hock, C. Martin, A.L. Barrett, E. Miller, M. Spowart, M. Howard, W. Ecklund, D. Carter, K. Gage and J. Wilson, 1994: The Integrated Sounding System: Description and preliminary observations from TOGA COARE. *Bull. Amer. Meteor. Soc.*, **75**, 553–567.

Pfister, L., K.R. Chan, T.P. Bui, S. Bowen, M. Legg, B. Gary, K. Kelly, M. Proffitt and W. Starr, 1993: Gravity waves generated by a tropical cyclone during the STEP tropical field program: A case study. *J. Geophys. Res.*, **98**, 8611–8637.

Ralph, F., M. Crochet and S. Venkateswaran, 1993: Obserbation of a mesoscale ducted gravity wave. *J. Atoms. Sci.*, **50**, 3277–3291.

Rotunno, R., J.B. Klemp and M.L. Weisman, 1988: A theory for strong, long-lived squall lines. *J. Atoms. Sci.*, **45**, 463–485.

Sato, K., 1997: Obsevational studies of gravity waves associated with convection. *Gravity Wave Processes*, Hamilton, K., Ed, NATO ASI Series, Springer, 63–68.

Schmidt, J.M. and W.R. Cotton, 1990: Interaction between upper and lower tropospheric gravity waves on squall line structure and maitenance. *J. Atoms. Sci.*, **47**, 1205–1222.

Shige, S. and T. Satomura, 1999: The gravity wave response in the troposphere around deep convection. *COARE 98 Proc. of a conference on the*

*TOGA Coupled Ocean-Atmosphere Response Experiment (COARE) (Boulder, CO, USA, 7–14 July 1998) (WMO/TD-No. 940)*, WCRP-107, 403–404.
Uccellini, L.W. and S.E. Koch, 1987: The synoptic setting and possible energy sources for mesoscale wave disturbances. *Mon. Wea. Rev.*, **115**, 721–729.
Webster, P.J. and R. Lukas, 1992: TOGA COARE: The coupled ocean-atmosphere response experiment. *Bull. Amer. Meteor. Soc.*, **73**, 1377–1416.

# TOGA-COARE IOP 期間中に熱帯対流圏下層で観測された周期1～2時間の擾乱

重　尚一[1]
（京都大学防災研究所）

TOGA-COARE IOP 期間中に連続稼働したウインドプロファイラーによって観測された鉛直流データを用い、熱帯対流圏下層の周期1～2時間の擾乱を検出した。鉛直流の平均振幅が約 0.1 m $s^{-1}$以上で、かつ数時間継続する7事例が確認された。

その内の1993年1月7日に Kapingamarangi（1.1°N, 154.8°E）で観測された周期60分で継続時間が6時間の1事例について詳しく解析した。観測された擾乱を重力波と仮定すると、鉛直波長は 5.4～7.6 km で、水平波長は 24～37 km であると推定された。さらに、この擾乱は、衛星画像と高層データの解析によって、Kapingamarangi から東南東約 400 km にあった線状メソスケール対流系によって励起され、対流圏内に形成された導波管内を水平伝播してきたと示唆された。

1　現所属：京都大学大学院理学研究科地球惑星科学専攻